



Article

Large-Separation Behavior of the Casimir–Polder Force from Real Graphene Sheet Deposited on a Dielectric Substrate

Galina L. Klimchitskaya ^{1,2,*} and Vladimir M. Mostepanenko ^{1,2,3}

¹ Central Astronomical Observatory at Pulkovo of the Russian Academy of Sciences, 196140 Saint Petersburg, Russia; vmostepa@gmail.com

² Peter the Great Saint Petersburg Polytechnic University, 195251 Saint Petersburg, Russia

³ Kazan Federal University, 420008 Kazan, Russia

* Correspondence: g.klimchitskaya@gmail.com

Abstract: The Casimir–Polder force between atoms or nanoparticles and graphene-coated dielectric substrates is investigated in the region of large separations. Graphene coating with any value of the energy gap and chemical potential is described in the framework of the Dirac model using the formalism of the polarization tensor. It is shown that the Casimir–Polder force from a graphene-coated substrate reaches the limit of large separations at approximately 5.6 μm distance between an atom or a nanoparticle and graphene coating independently of the values of the energy gap and chemical potential. According to our results, however, the classical limit, where the Casimir–Polder force no longer depends on the Planck constant and the speed of light, may be attained at much larger separations depending on the values of the energy gap and chemical potential. In addition, we have found a simple analytic expression for the Casimir–Polder force from a graphene-coated substrate at large separations and determined the region of its applicability. It is demonstrated that the asymptotic results for the large-separation Casimir–Polder force from a graphene-coated substrate are in better agreement with the results of numerical computations for the graphene sheets with larger chemical potential and smaller energy gap. Possible applications of the obtained results in nanotechnology and bioelectronics are discussed.

Keywords: Casimir–Polder force; graphene-coated substrate; asymptotic regime of large separations; classical limit



Citation: Klimchitskaya, G.L.; Mostepanenko, V.M. Large-Separation Behavior of the Casimir–Polder Force from Real Graphene Sheet Deposited on a Dielectric Substrate. *C* **2023**, *9*, 84. <https://doi.org/10.3390/c9030084>

Academic Editors: Ahmet Sinan Oktem and Matteo Strozzi

Received: 5 July 2023

Revised: 24 August 2023

Accepted: 27 August 2023

Published: 31 August 2023



Copyright: © 2023 by the authors. Licensee MDPI, Basel, Switzerland. This article is an open access article distributed under the terms and conditions of the Creative Commons Attribution (CC BY) license (<https://creativecommons.org/licenses/by/4.0/>).

1. Introduction

The Casimir–Polder force is a typical example of dispersion interactions caused by a fluctuating electromagnetic field which is zero in the mean but possesses a nonzero dispersion. Discovered by Casimir and Polder [1] as a relativistic generalization of the van der Waals interaction between two atoms (molecules) or an atom and a material surface, it has received wide recognition in both fundamental physics dealing with precision experiments and in nanotechnology (for more, see the monographs [2–7]).

The modern theoretical description of the Casimir–Polder force is based on quantum electrodynamics. In the original article [1], Casimir and Polder considered the interaction of two neutral atoms and an atom with an ideal metal plate. The case of an atom spaced at large separation from a plate made of real material characterized by the frequency-dependent dielectric permittivity was considered in [8]. This was done on the basis of the Lifshitz theory [9] describing the Casimir force acting between two thick plates by rarefying the material of one of them.

A more general formula for the potential energy of a molecule of solute in a dilute solution of low concentration as a function of the interface distance was obtained in [10] using the same rarefying procedure of one of the plates (see also [11]). At a later time, the Lifshitz formula for the Casimir–Polder interaction of microparticles with material plates was used in several hundreds papers (see [2–7] and references therein). This formula

allows calculation of the Casimir–Polder interaction given the dynamic atomic (molecular) polarizability and the dielectric permittivity of plate material. Formulas of this kind are applicable in the case of nanoparticles interacting with planar or gently curved surfaces under the condition that the nanoparticle radius R is much less than the distance to the surface [12–15].

Among the new materials which have appeared, the one-atom-thick layer of carbon atoms called graphene seems to hold the lead [16]. Thanks to its two-dimensional structure, graphene admits a theoretical description in the framework of the Dirac formalism of quantum electrodynamics [17,18] without resorting to the phenomenological assumptions and far-reaching extrapolations which are often used in condensed matter physics when dealing with ordinary three-dimensional materials. This enables the response of graphene to the electromagnetic field to be found as a function of frequency, wave vector, and temperature with the use of the polarization tensor [19–22]. In actual fact, the two independent components of the polarization tensor are equivalent to the spatially nonlocal dielectric permittivities of graphene [23,24]. Because of this, by using this formalism one can calculate the Casimir–Polder force acting from the source side of graphene on atoms, molecules, and nanoparticles.

Calculations of the Casimir–Polder force from graphene acting on atoms (see, e.g., [25–34]) and nanoparticles (see, e.g., [35–42]) find applications in both fundamental physics and nanotechnology. An expression for the force takes an especially simple form in the limiting case of large separations (high temperatures). At room temperature $T = 300$ K, this is reached at a few micrometers. In [43], the large separation behavior of the Casimir–Polder force was investigated for a graphene sheet with no foreign atoms possessing zero chemical potential and sufficiently small energy gap in the spectrum of quasiparticles.

Real graphene sheets are characterized by nonzero values of both the energy gap Δ and chemical potential μ . In a recent article [44], the large-separation behavior of the Casimir–Polder force was explored for a real graphene sheet freestanding in vacuum as a function of Δ and μ . It was shown that it is possible to control the force value by varying the values of Δ and μ and deal with the analytic asymptotic expressions for the force rather than with more complicated computations by means of the Lifshitz formula.

In practical implementations, graphene is usually deposited on a dielectric substrate. Here, we investigate the large-separation behavior of the Casimir–Polder force acting on atoms or nanoparticles from real graphene sheets characterized by an energy gap and chemical potential which are deposited on thick silica glass substrate. We find that the range of large separations for a graphene-coated substrate starts at approximately $5.6 \mu\text{m}$ from the surface and is almost independent of the values of Δ and μ . The ratio of forces from a graphene-coated substrate and an uncoated silica glass plate decreases with increasing Δ and increases with increasing μ . It is shown that the classical limit of the Casimir–Polder force from an ideal metal plane reached at the thermal length, for a graphene-coated substrate may be reached at much larger separations from the surface which essentially depend on the values of Δ and μ .

The analytic asymptotic expression for the large-separation behavior of the Casimir–Polder force from a graphene-coated substrate is found as a function of separation from the surface, energy gap, chemical potential, and temperature. The asymptotic results are compared with numerical computations of the Casimir–Polder force at large separations for different values of Δ and μ . According to our results, at some fixed separation an agreement between the asymptotic and numerical results becomes better with increasing chemical potential and worse with increasing energy gap. By and large, for a graphene-coated substrate the asymptotic results are found to be in slightly better agreement with the results of numerical computations than for a freestanding graphene sheet.

The structure of the article is as follows. Section 2 is devoted to the general formalism of the Lifshitz theory for graphene deposited on a substrate. In Section 3, we consider the impact of a substrate on the large-separation Casimir–Polder force from real graphene sheet. Section 4 is devoted to a confrontation between the analytic asymptotic results and

numerical computations in the presence of a substrate. Section 5 provides a discussion, while Section 6 lists our conclusions.

2. General Formalism

Here, we briefly present the formalism of the Lifshitz theory describing the Casimir–Polder force between an atom or a nanoparticle and any planar structure, e.g., a graphene-coated substrate, which are at temperature T and separated by a distance a . Using the dimensionless Matsubara frequencies $\zeta_l = 2a\zeta_l/c = 4\pi ak_B T l / (\hbar c)$, where k_B is the Boltzmann constant, $l = 0, 1, 2, \dots$, and $y = (4a^2 k_\perp^2 + \zeta_l^2)^{1/2}$ with $k_\perp = |\mathbf{k}_\perp|$, \mathbf{k}_\perp being the projection of the wave vector on the planar structure, the Lifshitz formula for the Casimir–Polder force takes the following form [6]:

$$F_{\text{sub}}(a, T) = -\frac{k_B T}{8a^4} \sum'_{l=0} \alpha_l \int_{\zeta_l}^{\infty} y dy e^{-y} \left[(2y^2 - \zeta_l^2) R_{\text{TM},l}(y) - \zeta_l^2 R_{\text{TE},l}(y) \right]. \quad (1)$$

In this equation, the prime on the summation sign divides the term with $l = 0$ by 2 and

$$\alpha_l = \alpha(i\zeta_l) = \alpha\left(i\frac{\zeta_l c}{2a}\right) \quad (2)$$

is the dynamic polarizability of an atom, a molecule, or a nanoparticle taken at a pure imaginary frequency that has the dimension of cm^3 .

Particular attention should be paid to the quantities $R_{\text{TM},l}$ and $R_{\text{TE},l}$ in (1); these are the reflection coefficients for the transverse magnetic (TM) and transverse electric (TE), or equivalently p and s, polarized electromagnetic waves on the planar structure calculated at the pure imaginary frequencies

$$\begin{aligned} R_{\text{TM},l}(y) &= R_{\text{TM}}(i\zeta_l, k_\perp) = R_{\text{TM}}\left(i\frac{\zeta_l c}{2a}, \frac{1}{2a}\sqrt{y^2 - \zeta_l^2}\right) = R_{\text{TM}}(i\zeta_l, y), \\ R_{\text{TE},l}(y) &= R_{\text{TE}}(i\zeta_l, k_\perp) = R_{\text{TE}}\left(i\frac{\zeta_l c}{2a}, \frac{1}{2a}\sqrt{y^2 - \zeta_l^2}\right) = R_{\text{TE}}(i\zeta_l, y). \end{aligned} \quad (3)$$

In our case, the planar structure is a graphene sheet deposited on a dielectric substrate. The electromagnetic response of the graphene is described by the polarization tensor in $(2 + 1)$ dimensions, whereas the material of the substrate reacts to the electromagnetic field through its frequency-dependent dielectric permittivity. The form of reflection coefficients in this unusual case was found in [45]. Using the dimensionless variables introduced above, these coefficients are provided by [29]

$$\begin{aligned} R_{\text{TM},l}(y) &= \frac{\varepsilon_l y (y^2 - \zeta_l^2) + \sqrt{y^2 + (\varepsilon_l - 1)\zeta_l^2} \left[y \tilde{\Pi}_{00,l}(y) - (y^2 - \zeta_l^2) \right]}{\varepsilon_l y (y^2 - \zeta_l^2) + \sqrt{y^2 + (\varepsilon_l - 1)\zeta_l^2} \left[y \tilde{\Pi}_{00,l}(y) + (y^2 - \zeta_l^2) \right]}, \\ R_{\text{TE},l}(y) &= \frac{(y^2 - \zeta_l^2) \left[y - \sqrt{y^2 + (\varepsilon_l - 1)\zeta_l^2} \right] - \tilde{\Pi}_l(y)}{(y^2 - \zeta_l^2) \left[y + \sqrt{y^2 + (\varepsilon_l - 1)\zeta_l^2} \right] + \tilde{\Pi}_l(y)}. \end{aligned} \quad (4)$$

Here, in analogy with (2), the dielectric permittivity of a substrate is taken at the pure imaginary frequencies

$$\varepsilon_l = \varepsilon(i\zeta_l) = \varepsilon\left(i\frac{\zeta_l c}{2a}\right). \quad (5)$$

The quantity $\tilde{\Pi}_{00,l}$ is the 00 component and $\tilde{\Pi}_l$ is the linear combination of components of the dimensionless polarization tensor

$$\tilde{\Pi}_{kn} = \frac{2a}{\hbar} \Pi_{kn}, \tag{6}$$

which are taken at the pure imaginary frequencies $i\zeta_l c / (2a)$.

The explicit expressions for the quantities $\tilde{\Pi}_{00,l}$ and $\tilde{\Pi}_l$ for real graphene sheets characterized by any value of the energy gap Δ and chemical potential μ are presented in [29]. Here, we use them in the more convenient identical form provided in [44]. Thus, the 00 component is

$$\begin{aligned} \tilde{\Pi}_{00,l}(y) = & \alpha \frac{y^2 - \zeta_l^2}{p_l} \Psi(D_l) + \frac{16\alpha a k_B T}{\tilde{v}_F^2 \hbar c} \ln \left[\left(e^{-\frac{\Delta}{2k_B T}} + e^{\frac{\mu}{k_B T}} \right) \left(e^{-\frac{\Delta}{2k_B T}} + e^{-\frac{\mu}{k_B T}} \right) \right] \\ & - \frac{4\alpha p_l}{\tilde{v}_F^2} \int_{D_l}^{\infty} du w_l(u, y) \operatorname{Re} \frac{p_l - p_l u^2 + 2i\zeta_l u}{[p_l^2 - p_l^2 u^2 + \tilde{v}_F^2 (y^2 - \zeta_l^2) D_l^2 + 2i\zeta_l p_l u]^{1/2}}. \end{aligned} \tag{7}$$

The quantity α in (7) is the fine structure constant

$$\alpha = \frac{e^2}{\hbar c} \approx \frac{1}{137}. \tag{8}$$

It should not be confused with the static polarizability α_0 used below. The function $\Psi(D_l)$ is defined as

$$\Psi(D_l) = 2 \left[D_l + (1 - D_l^2) \arctan \frac{1}{D_l} \right], \tag{9}$$

where

$$D_l \equiv D_l(y) = \frac{2a\Delta}{\hbar c p_l}, \quad p_l = p_l(y) = \sqrt{\tilde{v}_F^2 y^2 + (1 - \tilde{v}_F^2) \zeta_l^2} \tag{10}$$

and \tilde{v}_F is the dimensionless Fermi velocity, $\tilde{v}_F = v_F / c \approx 1/300$.

As to the function $w_l(u, y)$ entering (7), it is provided by

$$w_l(u, y) = \frac{1}{e^{B_l u + \frac{\mu}{k_B T}} + 1} + \frac{1}{e^{B_l u - \frac{\mu}{k_B T}} + 1}, \tag{11}$$

where

$$B_l \equiv B_l(y) = \frac{\hbar c p_l(y)}{4a k_B T}. \tag{12}$$

Using the same notations, we express the linear combination of the components of the polarization tensor $\tilde{\Pi}_l$ from Equation (4) defining the TE reflection coefficient [29,44]:

$$\begin{aligned} \tilde{\Pi}_l(y) = & \alpha (y^2 - \zeta_l^2) p_l \Psi(D_l) - \frac{16\alpha a k_B T \zeta_l^2}{\tilde{v}_F^2 \hbar c} \ln \left[\left(e^{-\frac{\Delta}{2k_B T}} + e^{\frac{\mu}{k_B T}} \right) \left(e^{-\frac{\Delta}{2k_B T}} + e^{-\frac{\mu}{k_B T}} \right) \right] \\ & + \frac{4\alpha p_l^2}{\tilde{v}_F^2} \int_{D_l}^{\infty} du w_l(u, y) \operatorname{Re} \frac{\zeta_l^2 - p_l^2 u^2 + \tilde{v}_F^2 (y^2 - \zeta_l^2) D_l^2 + 2i\zeta_l p_l u}{[p_l^2 - p_l^2 u^2 + \tilde{v}_F^2 (y^2 - \zeta_l^2) D_l^2 + 2i\zeta_l p_l u]^{1/2}}. \end{aligned} \tag{13}$$

As is seen from (1), (4)–(13), for computation of the Casimir–Polder force acting on some particle on the source side of a graphene-coated substrate, it is desirable to know the dynamic polarizability of this particle (2) and the dielectric permittivity of a substrate (5) within a sufficiently wide frequency region, along with the energy gap, the chemical potential of the graphene sheet, and the temperature.

It is pertinent to note that the above formalism was developed in the framework of the Dirac model of graphene [16–18], which applies when the energy is not too high, i.e., $\hbar\omega < 3$ eV [46]. Taking into consideration that the characteristic frequency of the Casimir–Polder force is provided by $c/(2a)$, which leads to energies of less than 1 eV at all separations exceeding 100 nm [6], it can be concluded that this formalism is very well adapted for theoretical description of the Casimir–Polder force at large separations.

3. Impact of Substrate on the Casimir–Polder Force from a Real Graphene Sheet at Large Separations

For a particle interacting with a lonely graphene sheet which is freestanding in vacuum, it was shown in [44] that, for separations exceeding some value a_0 from 2.3 to 3.2 μm , 99% of the total Casimir–Polder force is provided by the term of (1) with $l = 0$. This result is valid for various values of the energy gap and chemical potential of graphene. We start by finding how it is modified by the presence of a substrate.

For this purpose, we consider the term of (1) with $l = 0$

$$F_{\text{sub},0}(a, T) = -\frac{k_B T}{8a^4} \alpha_0 \int_0^\infty y^3 dy e^{-y} R_{\text{TM},0}(y), \tag{14}$$

where $\alpha_0 = \alpha(0)$ is the static polarizability of an atom or a nanoparticle. It is seen that $F_{\text{sub},0}$ does not depend on the TE reflection coefficient.

The reflection coefficient $R_{\text{TM},0}$ is obtained from (4), again by setting $l = 0$,

$$R_{\text{TM},0}(y) = \frac{\epsilon_0 y + \tilde{\Pi}_{00,0}(y) - y}{\epsilon_0 y + \tilde{\Pi}_{00,0}(y) + y}. \tag{15}$$

When obtaining (15), it was assumed that

$$\lim_{\zeta \rightarrow 0} \left[\zeta^2 \epsilon \left(i \frac{\zeta c}{2a} \right) \right] = 0, \tag{16}$$

which is valid for substrates made of both dielectric materials and metals described by the Drude model. The value of $\tilde{\Pi}_{00,0}(y)$ in (15) is provided by (7) with $l = 0$ [29]

$$\begin{aligned} \tilde{\Pi}_{00,0}(y) = & \frac{\alpha y}{\tilde{v}_F} \Psi(D_0) + \frac{16\alpha a k_B T}{\tilde{v}_F^2 \hbar c} \ln \left[\left(e^{-\frac{\Delta}{2k_B T}} + e^{\frac{\mu}{k_B T}} \right) \left(e^{-\frac{\Delta}{2k_B T}} + e^{-\frac{\mu}{k_B T}} \right) \right] \\ & - \frac{4\alpha y}{\tilde{v}_F} \int_{D_0}^{\sqrt{1+D_0^2}} du w_0(u, y) \frac{1-u^2}{\sqrt{1-u^2+D_0^2}}. \end{aligned} \tag{17}$$

Here, the quantity D_0 is obtained from (10) and B_0 entering w_0 is obtained from (12)

$$D_0 = \frac{2a\Delta}{\hbar c \tilde{v}_F y}, \quad B_0 = \frac{\hbar c \tilde{v}_F y}{4ak_B T}. \tag{18}$$

Note that Equation (14) of [44] for $\tilde{\Pi}_{00,0}$ contains a typo: the factor y^2 in the first term on the right-hand side of (14) in [44] should be replaced with y .

All numerical computations below are performed for a graphene sheet deposited on a fused silica glass (SiO_2) substrate. This substrate is typical in graphene technologies (see, e.g., [47–50]) and in precision measurements of the Casimir force from graphene [51,52]. The optical data for the complex index of refraction of fused silica glass can be found in [53] in the wide range of $\hbar\omega$ extending from 0.0025 eV to 2000 eV. The obtained dielectric permittivity of SiO_2 along the imaginary frequency axis is well known and has been used in many publications (see, e.g., [6]). It contains the two steps, one of which is due to

ionic polarization and another one is due to electronic polarization. The static dielectric permittivity of SiO₂ is $\epsilon_0 = 3.81$.

Now, we compute the large-separation Casimir–Polder force from a graphene-coated SiO₂ substrate using the full Lifshitz formula (1) and its term with $l = 0$ (14) for various values of the energy gap and chemical potential. Taking into account that in the presence of the substrate the region of large separations starts at separations exceeding a few micrometers, full computations using (1) can be safely performed by setting $\alpha_l \approx \alpha_0$ without sacrificing precision [6]. When using the Lifshitz formula (1), the computations are performed by (4)–(13). When Equation (14) is employed, we use (15), (17), and (18) in the computations. In both cases, we use the value of ϵ_0 for the SiO₂ substrate, and in full computations we use values of ϵ_l with $l \geq 1$.

Comparing the obtained results, we find that the full values of the Casimir–Polder force F_{sub} computed by (1) differ from the force $F_{\text{sub},0}$ computed by (14) in less than 1% at all separations $a \geq a_0 = 5.6 \mu\text{m}$ independently of the values of Δ and μ used in computations (see below for the typical specific values of these parameters). Thus, for a graphene sheet deposited on a substrate, the large-separation behavior of the Casimir–Polder force provided by $F_{\text{sub},0}$ is reached at larger separations than for a freestanding graphene sheet (i.e., from 2.3 to 3.2 μm , depending on the values of Δ and μ [44]). What is more, for a graphene-coated substrate the value of a_0 is essentially independent on Δ and μ . Note that for an uncoated silica glass plate the large-separation behavior of the Casimir–Polder force is reached at $a_0 = 6 \mu\text{m}$.

In an effort to determine the impact of graphene coating on the large-separation Casimir–Polder force, we computed the force $F_{\text{sub},0}$ from a graphene-coated SiO₂ substrate and $F_0^{\text{SiO}_2}$ from an uncoated fused silica plate. To compute the latter quantity, one should set $\tilde{\Gamma}_{00,0}(y) = 0$ in (15). In Figure 1a,b the computational results for the ratio $F_{\text{sub},0}/F_0^{\text{SiO}_2}$ at $T = 300 \text{ K}$, $a = 6 \mu\text{m}$ are shown as a function of the energy gap by (a) the four lines labeled 1, 2, 3, and 4 for $\mu = 0, 0.05, 0.1,$ and 0.15 eV , respectively, and (b) the three lines labeled 4, 5, and 6 for $\mu = 0.15, 0.2,$ and 0.25 eV , respectively. For illustrative purposes, the dashed lines show the value of the ratio $F_0^{\text{IM}}/F_0^{\text{SiO}_2}$ when the graphene-coated substrate is replaced with an ideal metal plane.

As seen in Figure 1a,b, the impact of graphene coating on the large-separation Casimir–Polder force increases with increasing chemical potential and decreasing energy gap of the graphene. As a result, the fused silica substrate coated by a graphene sheet with $\Delta = 0.1 \text{ eV}$ and $\mu = 0.25 \text{ eV}$ produces almost the same Casimir–Polder force at $a = 6 \mu\text{m}$ separation as an ideal metal plane.

It is well known that at separations above 6 μm the Casimir–Polder force from an ideal metal plane takes the so-called classical form, which does not depend on either \hbar or c [6]:

$$F_0^{\text{IM}}(a, T) = -\frac{3k_B T}{4a^4} \alpha_0. \quad (19)$$

In order to find how the large-separation Casimir–Polder force from a graphene-coated SiO₂ substrate approaches this classical limit depending on the values of Δ and μ , we can calculate the relative difference

$$\delta F_{\text{sub},0}(a, T) = \frac{F_{\text{sub},0}(a, T) - F_0^{\text{IM}}(a, T)}{F_0^{\text{IM}}(a, T)}. \quad (20)$$

In Figure 2, the computational results for $\delta F_{\text{sub},0}$ at $T = 300 \text{ K}$ are shown for a graphene coating with $\Delta = 0.2 \text{ eV}$ as a function of separation by the five lines labeled 1, 2, 3, 4, and 5 for $\mu = 0, 0.025, 0.05, 0.075,$ and 0.1 eV , respectively. The dashed line shows the lower boundary of the figure plane domain where the relative deviation between $F_{\text{sub},0}$ and F_0^{IM} is less than 1%.

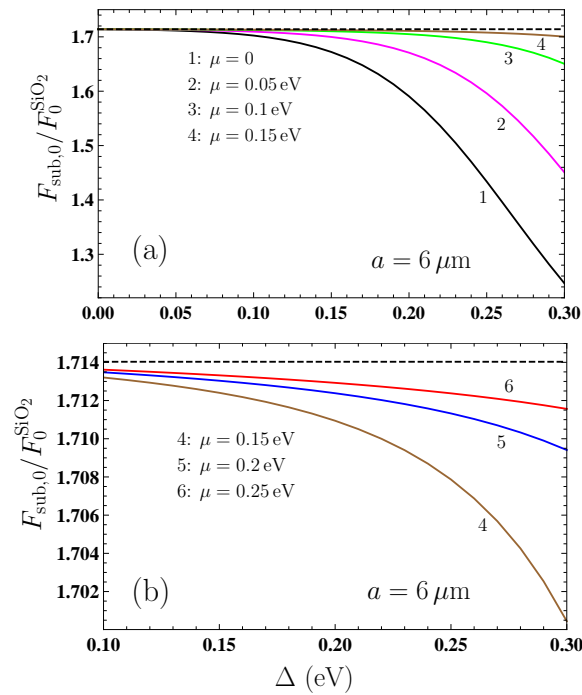


Figure 1. The ratio of the Casimir–Polder force from the graphene-coated SiO₂ substrate to that from an uncoated plate at the distance of 6 μm is shown as the function of the energy gap (a) by the lines labeled 1, 2, 3, and 4 for the chemical potential of graphene equal to 0, 0.05, 0.1, and 0.15 eV, respectively, and (b) by the lines labeled 4, 5, and 6 for the chemical potential equal to 0.15, 0.2, and 0.25 eV, respectively. The dashed lines show the ratio of the Casimir–Polder force from an ideal metal plane to that from an uncoated SiO₂ plate.

As is seen in Figure 2, for a graphene coating with $\mu = 0.1$ eV (line 5), the relative deviation (20) remains within 1% over the entire separation region $a > 5.6$ μm. As for the graphene coating with smaller $\mu = 0.075, 0.05, 0.025,$ and 0 eV, the Casimir–Polder force takes the classical form at larger separations equal to 6.5, 15.5, 35.5, and 53 μm, respectively. These values are only slightly larger than for a freestanding graphene sheet [44]. From Figure 2, it can be concluded that the Casimir–Polder force from a graphene-coated substrate takes the classical form at larger separations for graphene with lower chemical potential.

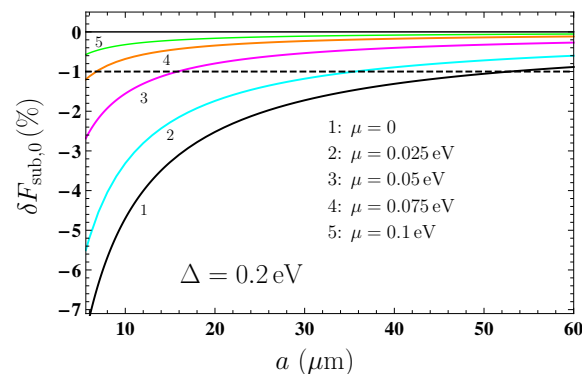


Figure 2. The relative difference between the large-separation Casimir–Polder forces from the graphene-coated SiO₂ substrate and an ideal metal plane for the energy gap of graphene equal to 0.2 eV at $T = 300$ K is shown as the function of separation by the lines labeled 1, 2, 3, 4, and 5 for the chemical potential of graphene equal to 0, 0.025, 0.05, 0.075, and 0.1 eV, respectively. The dashed line restricts the area of the figure plane where $\delta F_{\text{sub},0} \leq 1\%$.

In fact, for a graphene sheet deposited on a substrate, the initiation of an energy gap is almost unavoidable [16]. Thus, an energy gap equal to 0.3 eV is rather typical [51,52]. To cover this case, in Figure 3a,b we present the computational results for $\delta F_{\text{sub},0}$ at $T = 300$ K for a graphene coating with $\Delta = 0.3$ eV. These results are again shown as the function of separation (a) by the five lines labeled 1, 2, 3, 4, and 5 for $\mu = 0, 0.025, 0.05, 0.075,$ and 0.1 eV, respectively, over the separation interval from 5.6 to $60 \mu\text{m}$ and (b) by the four lines labeled 1, 2, 3, and 4 for $\mu = 0, 0.025, 0.05,$ and 0.075 eV, respectively, over the separation interval from 60 to $200 \mu\text{m}$. The dashed lines in Figure 3a,b again enclose the figure domain where $\delta F_{\text{sub},0}$ is less than 1%.

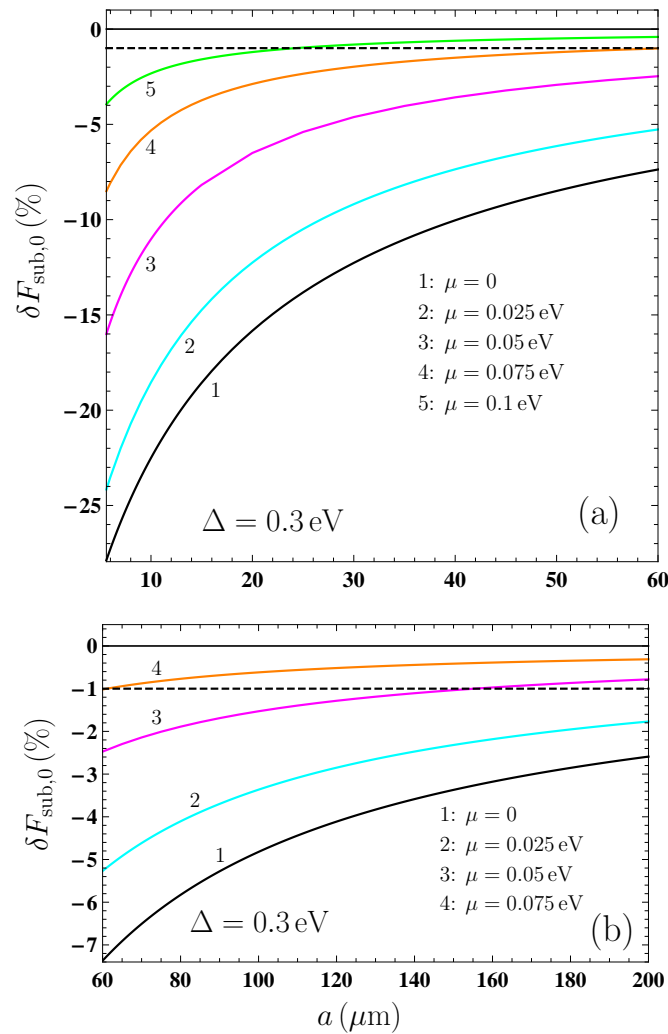


Figure 3. The relative difference between the large-separation Casimir–Polder forces from the graphene-coated SiO₂ substrate and an ideal metal plane for the energy gap of graphene equal to 0.3 eV at $T = 300$ K is shown as the function of separation (a) by the lines labeled 1, 2, 3, 4, and 5 for the chemical potential of graphene equal to 0, 0.025, 0.05, 0.075, and 0.1 eV, respectively, in the separation region from $5.6 \mu\text{m}$ to $60 \mu\text{m}$ and (b) by the lines labeled 1, 2, 3, and 4 for the chemical potential of graphene equal to 0, 0.025, 0.05, and 0.075 eV, respectively, in the separation region from $60 \mu\text{m}$ to $200 \mu\text{m}$. The dashed line restricts the areas of the figure plane where $\delta F_{\text{sub},0} \leq 1\%$.

As is seen in Figure 3a, only for a graphene coating with $\mu = 0.1$ eV (line 5) does the Casimir–Polder force take the classical form in the field of this figure (for $a > 24.5 \mu\text{m}$). Thus, with increasing energy gap the classical form of the force is reached at larger separations. From Figure 3b, it can be seen that for graphene sheets with $\mu = 0.075$ and 0.05 eV the Casimir–Polder force becomes classical starting from 63 and $157 \mu\text{m}$, respectively (lines 4

and 3). As for the graphene coating with $\mu = 0.025$ and 0 eV, the corresponding Casimir–Polder force does not take the classical form in the field of this figure up to $a = 200$ μm . Calculations show that the Casimir–Polder force from the graphene-coated substrate with $\Delta = 0.3$ eV, $\mu = 0.025$ and 0 eV becomes classical only at separations of 363 and 550 μm , respectively. By and large, Figures 2 and 3 demonstrate that with increasing μ the classical form of the Casimir–Polder force from the graphene-coated substrate is reached at shorter and with increasing Δ at larger separations.

4. Analytic Asymptotic Results Confronted with Numerical Computations in the Presence of Substrate

In this section, we obtain the analytic asymptotic expressions F_0^{as} for the large-separation Casimir–Polder force from a graphene-coated substrate $F_{\text{sub},0}$ and find the measure of agreement between F_0^{as} and the numerically computed $F_{\text{sub},0}$ for different values of the energy gap and chemical potential of a graphene sheet.

The asymptotic expression sought here is valid under the following condition:

$$\frac{2ak_B T}{\tilde{v}_F \hbar c} \gg 1, \tag{21}$$

which is satisfied with a large safety margin at $T = 300$ K, $a > 0.2$ μm (in fact, as was shown in Section 3, we consider separation distances exceeding 5.6 μm).

We consider the large-separation Casimir–Polder force (14) with the reflection coefficient (15) under the condition (21). This reflection coefficient can be rearranged to

$$R_{\text{TM}}(0, y) = 1 - \frac{2y}{\tilde{\Pi}_{00,0}(y) + (\epsilon_0 + 1)y}. \tag{22}$$

According to (17), the polarization tensor is of the order of parameter (21); thus, $\tilde{\Pi}_{00,0}(y) \gg 1$. What is more, the main contribution to the integral (14) is provided by $y \sim 1$. Because of these conditions, we can replace y with unity in the denominator of (22) and neglect $(\epsilon_0 + 1)$ in comparison with $\tilde{\Pi}_{00,0}(1)$. Therefore, (22) becomes

$$R_{\text{TM}}(0, y) \approx 1 - \frac{2y}{\tilde{\Pi}_{00,0}(1)}, \tag{23}$$

i.e., the TM reflection coefficient takes exactly the same approximate form as was found earlier for the freestanding graphene sheet [44].

After substitution of (23) in (14) and integration, the desired asymptotic expression takes the same form as in [44]

$$F_{\text{sub},0}^{\text{as}}(a, T) = F_0^{\text{as}}(a, T) = F_0^{\text{IM}}(a, T) \left[1 - \frac{8}{\tilde{\Pi}_{00,0}(1)} \right], \tag{24}$$

where $F_0^{\text{IM}}(a, T)$ is defined in (19).

The expression (24) should be supplemented by the approximate expression for $\tilde{\Pi}_{00,0}(1)$ found in [44] under the condition (21)

$$\begin{aligned} \tilde{\Pi}_{00,0}(1) \approx & \frac{16\alpha ak_B T}{\tilde{v}_F^2 \hbar c} \left[\ln \left(4 \cosh \frac{\Delta + 2\mu}{4k_B T} \cosh \frac{\Delta - 2\mu}{4k_B T} \right) \right. \\ & \left. - \frac{\Delta}{4k_B T} \left(\tanh \frac{\Delta + 2\mu}{4k_B T} + \tanh \frac{\Delta - 2\mu}{4k_B T} \right) \right]. \end{aligned} \tag{25}$$

We are coming now to a detailed comparison between the asymptotic expression for the Casimir–Polder force F_0^{as} provided by (24) and (25) and the numerically computed large-separation force $F_{\text{sub},0}(a, T)$ from a graphene-coated substrate using Equations (14), (15), and (17). This comparison can be made by considering the ratio $F_{\text{sub},0}/F_0^{\text{as}}$ for differ-

ent values of the graphene parameters. All computations are again performed at room temperature $T = 300$ K.

First, we consider an undoped graphene coating with $\mu = 0$ and compute the ratio $F_{\text{sub},0}/F_0^{\text{as}}$ for two different values of the energy gap $\Delta = 0.15$ eV and 0.2 eV. The computational results are shown in Figure 4 as the function of separation by the top and bottom solid lines, respectively. For comparison purposes, the ratio F_0/F_0^{as} for a freestanding graphene sheet (i.e., with no substrate) with the same values of Δ is plotted by the dashed lines.

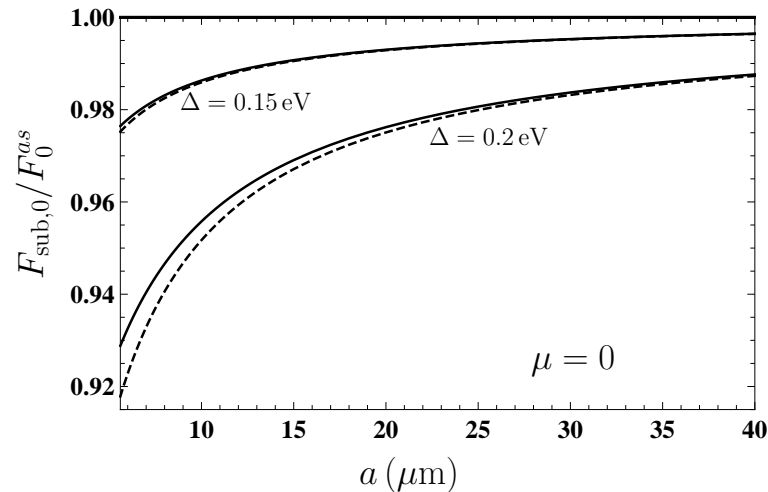


Figure 4. The ratio of the numerically computed large-separation Casimir–Polder force from the graphene-coated SiO₂ substrate to its asymptotic value for the zero chemical potential of graphene at $T = 300$ K is shown as the function of separation by the top and bottom solid lines for the energy gap equal to 0.15 and 0.2 eV, respectively. The similar ratio for the freestanding graphene sheets with the same parameters is shown by the dashed lines.

As seen in Figure 4, for a graphene coating with $\mu = 0$, $\Delta = 0.15$ eV, the asymptotic results reproduce the results of the numerical computations with better than 1% accuracy at separations exceeding 14.5 μm . With increasing energy gap, the accuracy of the asymptotic expressions becomes lower. Thus, for a graphene coating with $\mu = 0$, $\Delta = 0.2$ eV, the asymptotic expression is accurate within 1% starting from 25 μm separation. From Figure 4, it can be seen that in spite of the fact that the asymptotic expression used does not depend on the dielectric permittivity of a substrate it reproduces the results of numerical computations somewhat better than for a freestanding graphene sheet. This is illustrated by the solid lines, which lie slightly above the dashed ones.

Next, we consider a graphene coating with a reasonably large energy gap $\Delta = 0.2$ eV and consider the relationship between the asymptotic and numerical results for a large-separation Casimir–Polder force from a graphene-coated substrate for different values of the chemical potential. The computational results for the ratio $F_{\text{sub},0}/F_0^{\text{as}}$ in this case at $T = 300$ K are presented in Figure 5 by the three solid lines from bottom to top for the chemical potential equal to $\mu = 0.025$, 0.05, and 0.075 eV, respectively. The dashed lines show the ratio F_0/F_0^{as} for the freestanding graphene sheets with the same values of μ . In the inset, the two pairs of solid and dashed lines for $\mu = 0.05$ and 0.075 eV are reproduced on an enlarged scale within a narrower separation region for better visualization.

From Figure 5, it can be seen that with increasing μ the agreement between the asymptotic and numerically computed Casimir–Polder forces from the graphene-coated substrate becomes better. Thus, if for a graphene coating with $\mu = 0.025$ eV the 1% agreement is reached only at separations exceeding 41 μm , for $\mu = 0.05$ eV this measure of agreement is observed at $a > 13.5$ μm . As to the graphene coating with $\mu = 0.075$ eV, the better than 1% agreement between the asymptotic and numerical results holds over the entire range of large separations $a \geq 5.6$ μm . According to Figure 5 (see the inset as well), the solid lines lie above the dashed ones for all μ , i.e., the asymptotic expression (24) and

(25) is slightly more exact in the case of graphene-coated substrates than for freestanding graphene sheets.

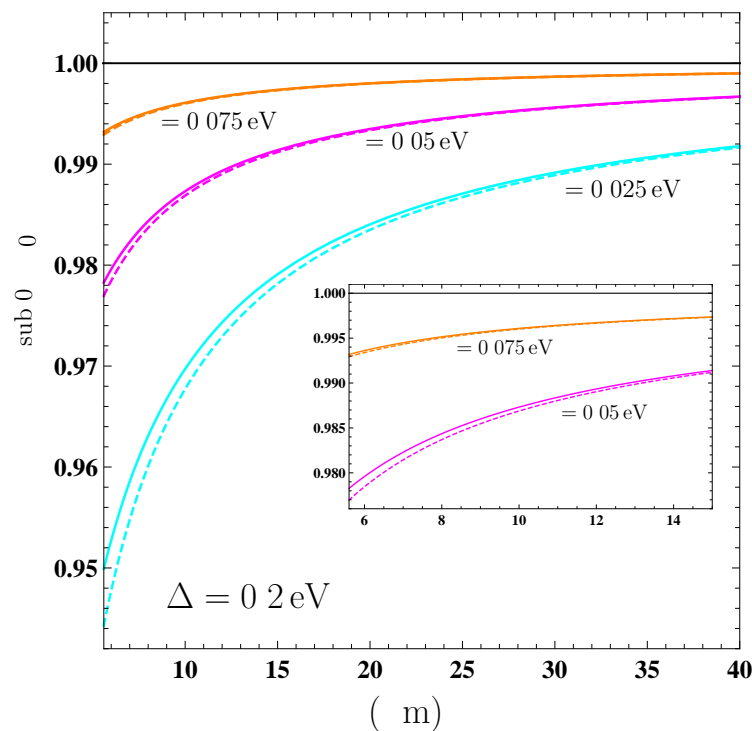


Figure 5. The ratio of the numerically computed large-separation Casimir–Polder force from the graphene-coated SiO₂ substrate to its asymptotic value for the energy gap of graphene equal to 0.2 eV at $T = 300$ K is shown as the function of separation by the three solid lines counted from bottom to top for the chemical potential equal to 0.025, 0.05, and 0.075 eV, respectively. The dashed lines show similar ratio for a freestanding graphene sheet with the same parameters. The region of short separations is reproduced in the inset on an enlarged scale for graphene sheets with a chemical potential of 0.05 eV (bottom) and 0.075 eV (top).

At the end of this section, we consider the case of a graphene coating with a larger energy gap $\Delta = 0.3$ eV, such as that used in the experiment measuring the Casimir force from a graphene-coated substrate in [51,52]. Here, we calculate the ratio $F_{\text{sub},0}/F_0^{\text{as}}$ over the wider range of μ up to $\mu = 0.25$ eV (the latter value was measured for the sample used in the experiment [51,52]). In Figure 6a,b, we present the computational results for this ratio at $T = 300$ K as a function of separation. The obtained results are shown by (a) the five lines labeled 1, 2, 3, 4, and 5 for $\mu = 0, 0.025, 0.05, 0.075,$ and 0.1 eV, respectively, over the separation interval from $5.6 \mu\text{m}$ to $100 \mu\text{m}$ and (b) by the three lines labeled 6, 7, and 8 for $\mu = 0.15, 0.2,$ and 0.25 eV, respectively, over the interval from 5.6 to $30 \mu\text{m}$.

As seen in Figure 6a, for lines 1, 2, and 3 (i.e., for the graphene coatings with $\mu = 0, 0.025,$ and 0.05 eV, respectively) the 1% agreement between the asymptotic and numerical results is not reached up to the separation of $100 \mu\text{m}$. As for the lines 4 and 5 ($\mu = 0.075,$ and 0.1 eV, respectively) the 1% agreement is reached at separation distances exceeding approximately 60 and $24 \mu\text{m}$. Thus, the agreement between the asymptotic and numerical results again becomes better with increasing value of the chemical potential.

From Figure 6b, an inference can be drawn that sufficiently large values of μ can fully compensate the negative role played by large Δ in an agreement between the asymptotic and numerical values of the large-separation Casimir–Polder force from graphene-coated substrates. According to Figure 6b, for all the three graphene coatings with $\mu = 0.15, 0.2,$ and 0.25 eV the asymptotic results are within 1% agreement with the results of numerical computations at all separations exceeding the border of the large-separation region equal to

5.6 μm . These results make possible the reliable use of the analytic asymptotic expression for the Casimir–Polder force from graphene-coated substrates with the proper combination of the values of Δ and μ .

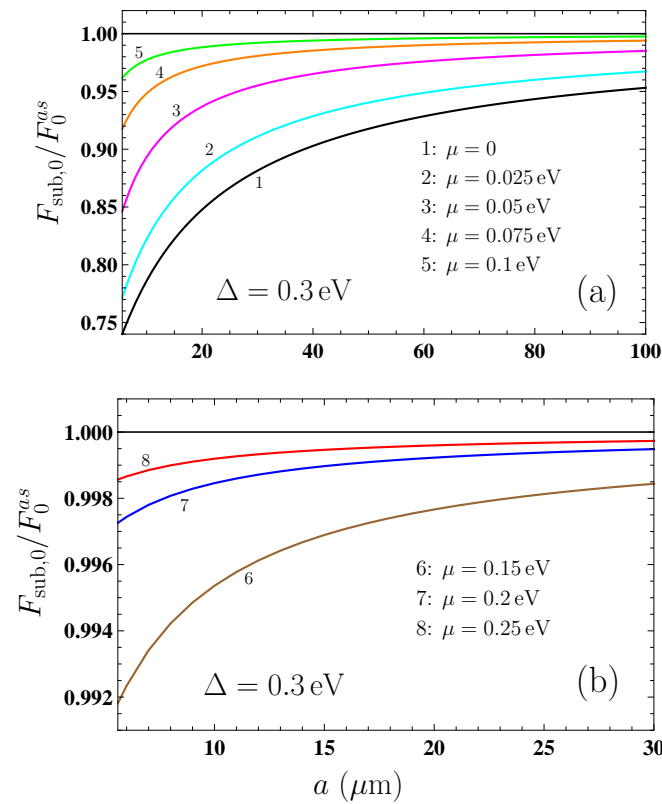


Figure 6. The ratio of the numerically computed large-separation Casimir–Polder force from the graphene-coated SiO_2 substrate to its asymptotic value for the energy gap of graphene equal to 0.3 eV at $T = 300$ K is shown as the function of separation by the solid lines counted from bottom to top (a) labeled 1, 2, 3, 4, and 5 for the chemical potential of graphene equal to 0, 0.025, 0.05, 0.075, and 0.1 eV, respectively and (b) labeled 6, 7, and 8 for the chemical potential equal to 0.15, 0.2, and 0.25 eV, respectively.

5. Discussion

The Casimir–Polder force considered in this paper is both a quantum and relativistic phenomenon which has no explanation on the basis of classical physics even in the case of atoms and nanoparticles interacting with conventional metallic and dielectric materials. It has been commonly believed, however, that at separations of a few micrometers the Casimir–Polder force takes its limiting form of large separations where it becomes classical and no longer depends on either the Planck constant or the speed of light.

The new two-dimensional material called graphene possesses many unusual properties. One of these properties is a giant thermal effect in the Casimir force at short separations, predicted in [54] and experimentally discovered in [51,52]. Another unusual property, first discussed in [44] using the simplified example of a freestanding graphene sheet in a vacuum, is that while the Casimir–Polder force between atoms, nanoparticles, and graphene reaches its limiting form of large separations at distances of 2–3 μm , this form may significantly deviate from being classical at distances up to tens of micrometers depending on the values of the energy gap and the chemical potential of graphene.

Here, we demonstrate that this unusual property is fully preserved in the case of graphene-coated dielectric substrates, which is of great physical significance. It is shown that although the limit of large separations for the Casimir–Polder force is reached at larger separations approximately equal to 5.6 μm in this case, the classical limit may be

reached at tens and even at hundreds of micrometers if the energy gap of the graphene coating is rather high and its chemical potential is rather low. As long as the classical limit is not reached, the Casimir–Polder force from a graphene-coated substrate depends on both the Planck constant and the speed of light, i.e., it remains a quantum and relativistic phenomenon. This effect is most pronounced in the application region of the analytic asymptotic expression in (24) and (25), which depends on both \hbar and c . By manufacturing graphene sheets with a small energy gap and sufficiently large chemical potential, it is possible to obtain the large-separation Casimir–Polder force from the graphene-coated substrate that is close to that from an ideal metal plane.

6. Conclusions

In the foregoing, we have analyzed the behavior of the Casimir–Polder force acting on atoms or nanoparticles from a graphene-coated substrate spaced at a separation of a few micrometers. We have shown that the limit of large separations is reached in this case at a distance of approximately 5.6 μm , which is almost independent on the energy gap and chemical potential of a graphene sheet. Although the limit of large separations is reached at a distance similar to that for conventional dielectric and metallic materials, we demonstrate that for graphene-coated substrates the Casimir–Polder force may attain the classical regime at much larger distances depending on the values of the energy gap and chemical potential of the graphene coating.

In addition, we find the analytic asymptotic expression for the Casimir–Polder force between atoms (nanoparticles) and graphene-coated substrates at large separations and determine the region of its applicability. The obtained expressions allow simple calculation of the Casimir–Polder force for substrates made of various materials and graphene coatings with any energy gap and chemical potential values.

The above results are derived in the framework of rigorous fundamental theory using the polarization tensor of graphene in the application region of the Dirac model. The results can be used in numerous applications of graphene in nanotechnology and bioelectronics, including such areas as field-effect transistors, interaction with lipid membranes, and graphene–semiconductor nanocomposites.

Funding: G.L.K. was partially funded by the Ministry of Science and Higher Education of the Russian Federation (“The World-Class Research Center: Advanced Digital Technologies”, contract No. 075-15-2022-311 dated 20 April 2022). The research of V.M.M. was partially carried out in accordance with the Strategic Academic Leadership Program “Priority 2030” of Kazan Federal University.

References

1. Casimir, H.B.G.; Polder, D. The influence of retardation on the London-van der Waals forces. *Phys. Rev.* **1948**, *73*, 360–372.
2. Mahanty, J.; Ninham, B.W. *Dispersion Forces*; Academic Press: London, UK, 1976.
3. Parsegian, V.A. *Van der Waals Forces: A Handbook for Biologists, Chemists, Engineers, and Physicists*; Cambridge University Press: Cambridge, UK, 2005.
4. Buhmann, S.Y. *Dispersion Forces*; Springer: Berlin/Heidelberg, Germany, 2012; Volumes 1–2.
5. Langbein, D. *Theory of Van der Waals Attraction*; Springer: Berlin/Heidelberg, Germany, 2013.
6. Bordag, M.; Klimchitskaya, G.L.; Mohideen, U.; Mostepanenko, V.M. *Advances in the Casimir Effect*; Oxford University Press: Oxford, UK, 2015.
7. Sernelius, B.E. *Fundamentals of van der Waals and Casimir Interactions*; Springer: New York, NY, USA, 2018.
8. Dzyaloshinskii, I.E.; Lifshitz, E.M.; Pitaevskii, L.P. The general theory of van der Waals forces. *Usp. Fiz. Nauk* **1961**, *73*, 381–422; Translated: *Adv. Phys.* **1961**, *10*, 165–209.
9. Lifshitz, E.M. The theory of molecular attractive forces between solids. *Zh. Eksp. Teor. Fiz.* **1955**, *29*, 94–110; Translated: *Sov. Phys. JETP* **1956**, *2*, 73–83.
10. Derjaguin, V.B.; Dzyaloshinsky, I.E.; Koptelova, M.M.; Pitaevsky, L.P. Molecular-Surface Forces in Binary Solutions. *Discuss. Faraday Soc.* **1965**, *40*, 246–252.
11. Parsegian, V.A. Formulae for the electrodynamic interaction of point particles with a substrate. *Molec. Phys.* **1974**, *27*, 1503–1511.
12. Kisylychyn, D.; Piatnytsia, V.; Lozovski, V. Electrodynamic interaction between a nanoparticle and the surface of a solid. *Phys. Rev. E* **2013**, *88*, 052403.
13. Sun, W. Interaction forces between a spherical nanoparticle and a flat surface. *Phys. Chem. Chem. Phys.* **2014**, *16*, 5846–5854.

14. Bimonte, G.; Emig, T.; Kardar, M. Casimir-Polder force between anisotropic nanoparticles and gently curved surfaces. *Phys. Rev. D* **2015**, *92*, 025028.
15. de Macedo, E.F.; Santos, N.S.; Nascimento, L.S.; Mathey, R.; Brenet, S.; de Moura, M.S.; Hou, Y.; Tada, D.B. Interaction between Nanoparticles, Membranes and Proteins: A Surface Plasmon Resonance Study. *Int. J. Mol. Sci.* **2023**, *24*, 591.
16. Aoki, H.; Dresselhaus, M.S. (Eds.) *Physics of Graphene*; Springer: Cham, Switzerland, 2014.
17. Castro Neto, A.H.; Guinea, F.; Peres, N.M.R.; Novoselov, K.S.; Geim, A.K. The electronic properties of graphene. *Rev. Mod. Phys.* **2009**, *81*, 109–162.
18. Katsnelson, M.I. *The Physics of Graphene*; Cambridge University Press: Cambridge, UK, 2020.
19. Bordag, M.; Fialkovsky, I.V.; Gitman, D.M.; Vassilevich, D.V. Casimir interaction between a perfect conductor and graphene described by the Dirac model. *Phys. Rev. B* **2009**, *80*, 245406.
20. Fialkovsky, I.V.; Marachevsky, V.N.; Vassilevich, D.V. Finite-temperature Casimir effect for graphene. *Phys. Rev. B* **2011**, *84*, 035446.
21. Bordag, M.; Klimchitskaya, G.L.; Mostepanenko, V.M.; Petrov, V.M. Quantum field theoretical description for the reflectivity of graphene. *Phys. Rev. D* **2015**, *91*, 045037; Erratum in *Phys. Rev. D* **2016**, *93*, 089907.
22. Bordag, M.; Fialkovskiy, I.; Vassilevich, D. Enhanced Casimir effect for doped graphene. *Phys. Rev. B* **2016**, *93*, 075414; Erratum in *Phys. Rev. B* **2017**, *95*, 119905.
23. Klimchitskaya, G.L.; Mostepanenko, V.M.; Sernelius, B.E. Two approaches for describing the Casimir interaction with graphene: density-density correlation function versus polarization tensor. *Phys. Rev. B* **2014**, *89*, 125407.
24. Klimchitskaya, G.L.; Mostepanenko, V.M. Quantum field theoretical framework for the electromagnetic response of graphene and dispersion relations with implications to the Casimir effect. *Phys. Rev. D* **2023**, *107*, 105007.
25. Chaichian, M.; Klimchitskaya, G.L.; Mostepanenko, V.M.; Tureanu, A. Thermal Casimir-Polder interaction of different atoms with graphene. *Phys. Rev. A* **2012**, *86*, 012515.
26. Kaur, K.; Kaur, J.; Arora, B.; Sahoo, B.K. Emending thermal dispersion interaction of Li, Na, K and Rb alkali-metal atoms with graphene in the Dirac model. *Phys. Rev. B* **2014**, *90*, 245405.
27. Klimchitskaya, G.L.; Mostepanenko, V.M. Impact of graphene coating on the atom-plate interaction. *Phys. Rev. A* **2014**, *89*, 062508.
28. Kaur, K.; Arora, B.; Sahoo, B.K. Dispersion coefficients for the interactions of the alkali-metal and alkaline-earth-metal ions and inert-gas atoms with a graphene layer. *Phys. Rev. A* **2015**, *92*, 032704.
29. Henkel, C.; Klimchitskaya, G.L.; Mostepanenko, V.M. Influence of the chemical potential on the Casimir-Polder interaction between an atom and gapped graphene or a graphene-coated substrate. *Phys. Rev. A* **2018**, *97*, 032504.
30. Khusnutdinov, N.; Kashapov, R.; Woods, L.M. Thermal Casimir and Casimir-Polder interactions in N parallel 2D Dirac materials. *2D Mater.* **2018**, *5*, 035032.
31. Klimchitskaya, G.L.; Mostepanenko, V.M. Nernst heat theorem for an atom interacting with graphene: Dirac model with nonzero energy gap and chemical potential. *Phys. Rev. D* **2020**, *101*, 116003.
32. Khusnutdinov, N.; Emelianova, N. The Low-Temperature Expansion of the Casimir-Polder Free Energy of an Atom with Graphene. *Universe* **2021**, *7*, 70.
33. Klimchitskaya, G.L. The Casimir-Polder interaction of an atom and real graphene sheet: Verification of the Nernst heat theorem. *Mod. Phys. Lett. A* **2020**, *35*, 2040004.
34. Klimchitskaya, G.L.; Mostepanenko, V.M. Casimir and Casimir-Polder Forces in Graphene Systems: Quantum Field Theoretical Description and Thermodynamics. *Universe* **2020**, *6*, 150.
35. Williams, G.; Kamat, P.V. Graphene-Semiconductor Nanocomposites: Excited-State Interactions between ZnO Nanoparticles and Graphene Oxide. *Langmuir* **2009**, *25*, 13869–13873.
36. Das, B.; Choudhury, B.; Gomathi, A.; Manna, A.K.; Pati, S.K.; Rao, C.N.R. Interaction of Inorganic Nanoparticles with Graphene. *ChemPhysChem* **2011**, *12*, 937–943.
37. Biehs, S.-A.; Agarwal, G.S. Anisotropy enhancement of the Casimir-Polder force between a nanoparticle and graphene. *Phys. Rev. A* **2015**, *90*, 042510; Erratum in *Phys. Rev. A* **2015**, *91*, 039901.
38. Devi, J.M. Simulation Studies on the Interaction of Graphene and Gold Nanoparticle. *Int. J. Nanosci.* **2018**, *17*, 1760043.
39. Low, S.; Shon, Y.-S. Molecular interactions between pre-formed metal nanoparticles and graphene families. *Adv. Nano Res.* **2018**, *6*, 357–375.
40. Huang, L.-W.; Jeng, H.-T.; Su, W.-B.; Chang, C.-S. Indirect interactions of metal nanoparticles through graphene. *Carbon* **2021**, *174*, 132–137.
41. Klimchitskaya, G.L.; Mostepanenko, V.M.; Tsybin, O.Yu. Casimir-Polder attraction and repulsion between nanoparticles and graphene in out-of-thermal-equilibrium conditions. *Phys. Rev. B* **2022**, *105*, 195430.
42. Klimchitskaya, G.L.; Korikov, C.C.; Mostepanenko, V.M.; Tsybin, O.Yu. Impact of Mass-Gap on the Dispersion Interaction of Nanoparticles with Graphene out of Thermal Equilibrium. *Appl. Sci.* **2023**, *13*, 7511.
43. Klimchitskaya, G.L.; Mostepanenko, V.M. Classical Casimir-Polder force between polarizable microparticles and thin films including graphene. *Phys. Rev. A* **2014**, *89*, 012516.
44. Klimchitskaya, G.L.; Mostepanenko, V.M. Casimir-Polder Force on Atoms or Nanoparticles from the Gapped and Doped Graphene: Asymptotic Behavior at Large Separations. *C- Carbon Res.* **2023**, *9*, 64.
45. Klimchitskaya, G.L.; Mohideen, U.; Mostepanenko, V.M. Theory of the Casimir interaction from graphene-coated substrates using the polarization tensor and comparison with experiment. *Phys. Rev. B* **2014**, *89*, 115419.

46. Zhu, T.; Antezza, M.; Wang, J.-S. Dynamical polarizability of graphene with spatial dispersion. *Phys. Rev. B* **2021**, *103*, 125421.
47. Hong, S.-Y.; Dadap, J.I.; Petrone, N.; Yeh, P.-C.; Hone, J.; Osgood, Jr., R.M. Optical Third-Harmonic Generation in Graphene. *Phys. Rev. X* **2013**, *3*, 021014.
48. Li, H.; He, P.; Yu, J.; Lee, L.J.; Yi, A.Y. Localized rapid heating process for precision chalcogenide glass molding. *Opt. Lasers Engineer.* **2015**, *73*, 62–68.
49. Marchena, M.; Song, Z.; Senaratne, W.; Li, C.; Liu, X.; Baker, D.; Ferrer, J.C.; Mazumder, P.; Soni, K.; Lee, R.; Pruneri, V. Direct growth of 2D and 3D graphene nano-structures over large glass substrates by tuning a sacrificial Cu-template layer. *2D Mater.* **2017**, *4*, 025088.
50. Yuan, Y.; Wang, Y.; Liu, S.; Zhang, X.; Liu, X.; Sun, C.; Yuan, D.; Zhang, Y.; Cao, X. Direct chemical vapor deposition synthesis of graphene super-hydrophobic transparent glass. *Vacuum* **2022**, *202*, 111136.
51. Liu, M.; Zhang, Y.; Klimchitskaya, G.L.; Mostepanenko, V.M.; Mohideen, U. Demonstration of Unusual Thermal Effect in the Casimir Force from Graphene. *Phys. Rev. Lett.* **2021**, *126*, 206802.
52. Liu, M.; Zhang, Y.; Klimchitskaya, G.L.; Mostepanenko, V.M.; Mohideen, U. Experimental and theoretical investigation of the thermal effect in the Casimir interaction from graphene. *Phys. Rev. B* **2021**, *104*, 085436.
53. Palik, E.D. (Ed.) *Handbook of Optical Constants of Solids*; Academic Press: New York, NY, USA, 1985.
54. Gómez-Santos, G. Thermal van der Waals interaction between graphene layers. *Phys. Rev. B* **2009**, *80*, 245424.

Disclaimer/Publisher’s Note: The statements, opinions and data contained in all publications are solely those of the individual author(s) and contributor(s) and not of MDPI and/or the editor(s). MDPI and/or the editor(s) disclaim responsibility for any injury to people or property resulting from any ideas, methods, instructions or products referred to in the content.